PCCP

The mechanism and rate constants for oxidation of indenyl radical C9H7 with molecular oxygen O2: A theoretical study

Journal:	*Physical Chemistry Chemical Physics*
Manuscript ID	CP-ART-02-2019-001122.R2
Article Type:	Paper
Date Submitted by the Author:	29-Mar-2019

Complete List of Authors:	Ghildina, Anna; Samara University Porfiriev, Denis; Samara University Azyazov, Valeriy; Samara National Research University; Lebedev Physical Institute of RAS, Department of Chemical & Electric Discharge Lasers Mebel, Alexander; Florida International University, Chemistry and Biochemistry

The mechanism and rate constants for oxidation of indenyl radical C_9H_7 with molecular oxygen O_2: A theoretical study

A. R. Ghildina,[1,2] D. P. Porfiriev,[1,2] V. N. Azyazov,[1,2,*] and A. M. Mebel[1,3,†]

[1] Samara University, Samara, 443086, Russia

[2] Lebedev Physical Institute, Samara, 443011, Russia

[3] Department of Chemistry and Biochemistry, Florida International University, Miami, FL 33199, USA

Abstract. Ab initio G3(MP2,CC)//B3LYP/6-311G(d,p) calculations have been carried out to map out the $C_9H_7O_2$ potential energy surface in relation to the reaction of 1-indenyl radical with molecular oxygen. The resulting energetics and molecular parameters of the species involved in the reaction have been then utilized in Rice-Ramsperger-Kassel-Marcus Master Equation calculations of temperature- and pressure-dependent reaction rate constants and product branching ratios. The results demonstrate that, while the reaction is insignificant at low temperatures, at higher temperatures, above 800 K or higher depending on pressure, the prevailing reaction channel leads to the formation of the 1-H-inden-1-one + OH products via a 1,3-H shift from C to O in the initial association complex W1 accompanied by OH elimination through a high barrier of 25.6 kcal/mol. The branching ratio of 1-H-inden-1-one + OH increases from ~61% to ~80% with temperature, whereas *c*-C_6H_4-CH_2CHO + CO (32-12%) and coumarin + H (7-6%) are significant minor products. The total rate constant of the indenyl + O_2 reaction leading to the bimolecular products is independent of pressure and exceeds 1.0×10^{-15} cm^3 $molecule^{-1}$ s^{-1} only at temperatures above 2000 K reaching 6.7×10^{-15} cm^3 $molecule^{-1}$ s^{-1} at 2500 K. The indenyl + O_2 reaction is concluded to be too slow to play a substantial role in oxidation of the five-member ring in indenyl and the present results corroborate the assertion that molecular oxygen is not an efficient oxidizer of five-member-ring radicals.

* E-mail: azyazov@ssau.ru
† E-mail: mebela@fiu.edu

1. Introduction

Polycyclic aromatic hydrocarbons (PAH), which are produced in incomplete combustion of fossil fuels and biomass from natural processes, are considered among the most abundant pollutants and soot precursors, which exert a great impact on the environment and health.[1–3] In this regard, PAH and soot formation is one of the "hottest" subjects in the current combustion research.[4-14] The chemical mechanisms for PAH and soot formation and degradation in combustion are presented by a large variety of reactions between molecules and radicals in different isomeric forms.[1,2,15-19] The growth of the simplest aromatic hydrocarbons is an important link in the formation of large PAHs and soot precursors. With the increase of molecular weight of PAHs, their toxicity generally increases.[20] The significant role of 1-indenyl radical C_9H_7 in the process of PAH formation is identified in many works. [15, 20,21-26] Besides its ability to recombine with the abundant cyclopentadienyl radical, C_5H_5, to form carcinogenic phenanthrene at high temperatures, [20, 27-29] the parent molecule of the radical, indene, consisting of two aromatic six- and five-member rings causes a toxic effect by itself.

A number of previous experimental and theoretical studies paid attention to chemical pathways of the formation of indene under combustion conditions,[25,30-32] but the information about its degradation in combustion environments, in particular, through oxidation of its most stable, resonantly stabilized radical, 1-indenyl, formed after an H atom abstraction from the CH_2 group in the five member ring, remains scarce. In a series of previous works,[33-37] we investigated potential energy surfaces (PES), reaction mechanism and kinetics for the oxidation of an isolated five-member ring, cyclopentadienyl radical C_5H_5, with the common oxidants such as O_2, O, and OH, abundant in the combustion environment.[2,19] Our studies built upon previous theoretical calculations by Zhong and Bozzelli[38] and Robinson and Lindstedt[39] but used up-to-date methods of electronic structure capable to provide chemical accuracy for reaction intermediates and transition states within ~1 kcal/mol combined with the Rice-Ramsperger-Kassel-Marcus Master Equation (RRKM-ME) approach to evaluate temperature- and pressure dependent reaction rate constants and relative yields of various products. The higher-level energy and the a priori RRKM-ME calculations allowed us to generate reaction rate constants, which are expected to be close to 'kinetic accuracy', i.e., with accuracy comparable to the experimental one.[40] However, in order to understand the oxidation mechanism of larger PAHs and soot, C_5H_5 may not be the most appropriate model. It is important to study how the oxidation mechanism of the five-member ring changes when such a ring is combined with six-member rings in PAH molecules or is embedded on the surface of a soot particle. In this view, the oxidation behavior of the 1-indenyl radical (or merely indenyl from here on), which represents the simplest radical where one six- and one five-member rings are joined together, should be informative. Frenklach and

co-workers[16] recently proposed a kinetic model for soot growth and oxidation considering the processes occurring on the soot particle surface site, which gives an order of magnitude agreement with experiment in laminar diffusion and partially premixed flames.[41-44] The principle oxidation mechanism was identified to be the formation of oxyradicals, their decomposition, formation of hard-to-oxidize embedded five-member rings, and oxidation of the latter predominantly by O atoms. The analysis showed O as the most effective oxidizer of the embedded five-member rings, which controls the rate of the overall oxidation. The model predicted fast oxidation during a brief initial period followed by a slow-oxidation one related to the oxidation of five-member rings. In the meantime, accurate kinetic data on the oxidation of embedded five-member rings on sterically different surface sites are not yet available. In order to improve the oxidation kinetic models, one needs to unravel the reaction mechanism of five-member rings on a PAH edge (with a different extent of embedment) with O_2, O, OH, and O_2H, and the studies of indenyl reactions with these oxidizers represent important first steps on this path.

To our knowledge, the only study addressing the indenyl (C_9H_7) + O_2 reaction is the work by Lindstedt et al.[15] who characterized the PES for the oxidation pathways using the G3MP2B3 method and employed the RRKM/ME approach and variable transition state theory to evaluate rate constants for the C_9H_7 + O_2/HO_2 systems. In particular, they identified several reaction channels for C_9H_7 + O_2 with products being C_6H_5O + C_3H_2O, C_7H_7 + CO + CO, and C_7H_6O + C_2HO. Rate constants were calculated within the assumption that all channels can be modeled as one-step processes with the slowest step prior to the break- up of the five-member ring controlling the reaction rate for each channel.[15] However, the computed PES was far from complete and, most importantly, did not cover the OH elimination channel analogous to cyclopentadienone + OH, which was recently demonstrated to be the major reaction channel for the prototype C_5H_5 + O_2 reaction.[33] In this view, a careful re-examination of the PES, mechanism, and kinetics of the C_9H_7 + O_2 reaction is warranted and required. Thus, the goal of the present paper is to map out the PES for indenyl + O_2 using high-level density functional and *ab initio* calculations and to utilize the PES data in multichannel-multiwell RRKM-ME calculations of temperature- and pressure-dependent rate constants and product branching ratios.

2. Theoretical methods

Rate constant calculations require accurate energies, structures and molecular parameters (rotational constants and vibrational frequencies) for reaction intermediates and transition states involved in the reaction. Geometries of all relevant species on the $C_9H_7O_2$ PES were optimized here at the hybrid density functional B3LYP/6-311G(d,p) level of theory.[45,46] Vibrational

frequencies were computed at the same theoretical level and were used to evaluate zero-point vibrational energy corrections (ZPE). Intrinsic reaction coordinate (IRC) calculations were performed to confirm connections between transition states and local minima. The refinement of single-point energies was carried out employing the modified G3(MP2,CC)//B3LYP/6-311G(d,p)[47,48] composite scheme where the energies were computed as

$$\mathrm{E_0[G3(MP2,CC)] = E\left[CCSD(T)/6-311G^{**}\right] + \Delta E_{MP2} + E(ZPE)}$$

Here $\mathrm{\Delta E_{MP2} = E[MP2/G3Large] - E\left[MP2/6-311G^{**}\right]}$ is a basis set correction and E(ZPE) is the zero-point energy. In the CCSD(T) and MP2 calculations for open-shell species, the energies were computed from restricted RHF-RCCSD(T) and unrestricted UMP2 energy values, respectively, where RHF-RCCSD(T) here denotes partially spin-adapted open-shell coupled cluster singles and doubles theory augmented with a perturbation correction for triple excitations starting from molecular orbitals, obtained from restricted open shell Hartree−Fock (ROHF) calculations. The electronic structure calculations were performed using the GAUSSIAN 09[49] and MOLPRO 2010[50] program packages.

The a priori RRKM-ME calculations, which can ensure 'kinetic accuracy' given reliable geometric and energy data,[40] were carried out by the Master Equation System Solver (MESS) package.[51,52] The Master Equation approach[53] takes into account chemical processes occurring at fixed energy, including isomerizations between multiple different wells on a PES, dissociations from each well to the products, dissociation back to bimolecular reactants, and bimolecular association. These microcanonical rate constants are normally computed using transition state theory (TST) for a unimolecular process, as in RRKM theory, where a rate constant $k(E)$ at an internal energy E for a unimolecular reaction $A^* \rightarrow A^{\#} \rightarrow P$ is expressed as

$$k(E) = \kappa \frac{\sigma}{h} * \frac{W^{\neq}(E - E^{\neq})}{\rho(E)},$$

where κ is the transmission coefficient accounting for quantum effects, such as tunneling and non-classical reflection, σ is the reaction path degeneracy, h is Plank's constant, $W^{\#}(E\text{-}E^{\#})$ denotes the total number of states for the transition state (activated complex) $A^{\#}$ with a barrier $E^{\#}$, $\rho(E)$ represents the density of states of the energized reactant molecule A*, and P is the product or products. Here, the Rigid-Rotor, Harmonic-Oscillator (RRHO) model was generally utilized in the calculations of the densities of states for the local minima and the number of states for the transition states. Tunneling corrections using asymmetric Eckart potentials were included in rate constant calculations.

The importance of considering the rate constants dependence on pressure is explained by the necessity to describe the kinetics under high-pressure conditions. Even when the total rate constant is only weakly pressure-dependent, the branching amongst different product channels often is still strongly dependent on pressure, which can profoundly affect the operative reaction pathways.[30] In order to take into account the effect of pressure, the master equation treatment considers inelastic collisions with a bath gas leading to transitions in energy within each well. These 'vertical' transition rates are typically modeled as a product of a Lennard-Jones collision rate Z and an energy transfer probability $P(E',E)$ that decays exponentially with the energy of the transition. Here, the "exponential down" model[54] was utilized to describe this probability, with the temperature dependence of the range parameter α for the deactivating wing of the energy transfer function expressed as $\alpha(T) = \alpha_{300}(T/300\ \mathrm{K})^n$, with $n = 0.7$ and $\alpha_{300} = 333\ \mathrm{cm}^{-1}$. The Lennard-Jones parameters were taken as ($\varepsilon/\mathrm{cm}^{-1}$, σ/Å) = (230, 4.01). These collision parameters were deduced by Jasper and Hansen for the methylcyclopentadienyl radical ($C_5H_4CH_3$) + Kr reaction[55] and were earlier used by us for the analogous prototype $C_5H_5 + O_2$ system.[33] As has been shown earlier by Jasper and Miller,[56] results for other heavy atomic and diatomic baths are likely to be very similar to those for Kr, with differences within the accuracy of the approach for predicting collisional energy transfer parameters for master equation calculations.

The solution of the master equation directly yields time dependent populations and energy distributions within each well. The numerical time dependent populations need to be converted to the phenomenological rate constants describing the overall processes occurring on the PES. While being robust in simple cases (like when only a single well is present), theoretical methods to carry out such conversion become ambiguous due to the blurring of time scales for different processes, especially at high temperatures and for reactions with multiple wells. The time dependence represented by an expansion in the eigensolution for the transition matrix directly correlates with that inferred from the phenomenological rate equation but this correlation strongly depends on a clear separation of time scales/eigenvalues into those for the slow chemical processes (chemically significant eigenvalues, CSEs) and those for the fast energy relaxation (internal energy relaxation eigenvalues, IEREs).[53] The MESS package employed in the present work is specifically designed as a master equation solver for complex-forming chemical reactions with multiple wells and bimolecular products and uses an alternative formulation of the master equation in which the dynamical phase space consists of only the microscopic populations of the various isomers constituting the reactive complex, whereas the bimolecular reactants and products are treated equally as sources and sinks.[52] In order to alleviate the issue of blurring between CSEs and IEREs, this

reformulated method employs the technique of 'merging' different isomers into one species as soon as they equilibrate on the timescale comparable to that of the energy relaxation. For instance, when some of the chemical eigenvalues approach the energy relaxation limit, the equilibration between the corresponding groups of species occurs so rapidly that it cannot be separated from the energy relaxation processes. The corresponding eigenstates are then considered as effectively relaxational ones and the effective number of species is reduced. The species in equilibrium with each other are then united and treated as one, with the dimensionality of the effective chemical subspace also been reduced. Equilibration/merging between the reactive complex isomers and bimolecular reactants/products is taken into account as well. The MESS package automatically merges isomers and bimolecular species at a particular temperature and pressure whenever necessary, based on the relationship between CSEs and IEREs.

3. Results and discussion

3.1. Potential energy surface

The initial structure of the reactants - the indenyl radical and molecular oxygen are shown in Figure 1. After the initial attachment of O_2 to the C2 position in the five-membered ring of indenyl forming intermediate W1 via a low barrier of 2.8 kcal/mol (all the energies are given relatively to the initial reactants), three possible pathways were found – the first one (Figure 2) – where the O atom of O_2, which is not connected to C2, migrates toward C3 to form intermediate W2. W2 further isomerizes through ring opening C2-C3 via a barrier of 27.2 kcal/mol at transition state TS2-3 producing W3, residing in a deep potential well of 81.5 kcal/mol. After this critical barrier is overcome, the reaction proceeds via closure of a six-member ring containing an oxygen atom to W4, H migration from C2 to the out-of-ring O atom making W5, ring opening to W6, H migration from OH to the C_2H_2 side chain forming W7, and finally, CO_2 elimination producing ortho-vinyl phenyl radical P1. The barrier at TS5-6 for the reverse ring closure from W6 to W5 is calculated to be only 0.9 and 0.3 kcal/mol at the B3LYP and CCSD(T) levels of theory, respectively, and further G3(MP2,CC) calculations give the energy of the transition state lower than that of W6. This result indicates that W6 is at best a metastable structure and for the reaction consideration, the W5 $\rightarrow$ W7 rearrangement involving the ring opening and 1,6-H shift from OH to C_2H_2 can be treated as a single step. The overall exothermicity of the indenyl + O_2 $\rightarrow$ ortho-vinyl phenyl + CO_2 reaction channel is 67.2 kcal/mol at our highest G3(MP2,CC) level of theory that is similar to the exothermicity of the C_5H_5 + O_2 $\rightarrow$ 1,3-butadien-1-yl (C_4H_5) + CO_2 reaction, 68.3 kcal/mol, computed earlier at the CCSD(T)-F12/cc-pVTZ-f12 level.[33]

The second reaction pathway is initiated by the attachment of O_2 to the C2 position as well, but from W1, the outer O atom moves toward the C1 position in the ring (Fig. 2) through TS1-8 via a barrier of 18.6 kcal/mol relative to the initial reactants, which is 5.6 kcal/mol higher than that at TS1-2. After intermediate W8 is formed, it rearranges, through the C1-C2 bond cleavage, to isomer W9 which is located in a potential well 63.7 kcal/mol deep. The further mechanism of the reaction is similar to the first pathway and includes the ring closure to W10 through a 18.5 kcal/mol barrier at TS9-10, then the migration of the H atom from C2 to the out-of-ring O atom forming W11 via a 49.5 kcal/mol barrier at TS10-11. Subsequent ring opening via TS11-12 with a barrier of 26.0 kcal/mol produces W12, and a further sequence of low-barrier fast reaction steps including migration of the H atom followed by CO_2 elimination leads to the styrenyl radical C_8H_7 + CO_2 products, P2, exothermic by 68.7 kcal/mol.

On the third two-step pathway, the indenyl + O_2 reaction leads to the 1-H-inden-1-one C_9H_6O product P3 through OH elimination (Fig. 2). This route also begins with the formation of W1 and is followed by 1,3-H migration from C2 to the outer oxygen atom accompanied with the cleavage of the O-O bond splitting the OH group with the formation of 1-H-inden-1-one through a transition state TS1-P3 residing 25.6 kcal/mol above the reactants. IRC calculations confirmed direct connection of TS1-P3 with C_9H_6O + OH and W1 in forward and reverse directions, respectively. This reaction channel is analogous to the cyclopentadienone + OH channel in the C_5H_5 + O_2 reaction which proved to be the dominant product channel at combustion temperatures.[33]

Additionally, we considered here the reaction pathways leading from the low-energy intermediates W3 and W9 to different products including H, CO, HCO, HCCO, and C_3H_2O eliminations. Some of these channels were earlier proposed by Lindstedt and co-workers.[15] Table 1 shows a comparison between the relative energies of various intermediates and transition states which were considered in both studies. Normally, the agreement is within 2-3 kcal/mol with a few exceptions usually related to the fact that here we investigated an array of different conformations for various isomers and found lower energy conformations than those considered in the previous study. Let us begin with the pathways originating from W3 (Figure 3). As confirmed by IRC calculations, a direct H loss from the CHCHO side chain in W3 is accompanied with the ring closure and leads to the formation of 3H-isochromen-3-one P4 via a high barrier of 58.3 kcal/mol at TS3-P4. The most favorable CO loss pathway, W3 $\rightarrow$ W14 $\rightarrow$ W15 $\rightarrow$ P5 + CO, involves *cis-trans* isomerization of the CHCHO side chain followed by the H transfer from the other HCO side chain to the α-carbon of CHCHO and elimination of the remaining CO group. The product P5, *c*-$C_6H_4CH_2CHO$, is a radical originating from 2-phenylacetaldehyde with an H atom removed in the ortho position in the ring. The overall

exothermicity of the indenyl + O_2 → P5 + CO reaction is 48.2 kcal/mol and the highest barrier along this pathway is found at TS15-P5, which resides 33.9 kcal/mol above W3. Intermediate W15 can also dissociate to (6-methylenecyclohexa-2,4-dienylidene)methanone P6 by elimination of the HCO radical, but this channel is significantly less favorable than the CO loss to P5. Other CO elimination channels involve 1,2-H shifts from the HCO group in one of the two side chains of W3 accompanied with or followed by the C-C bond cleavage. For instance, when the shorter HCO side chain participates in the reaction, this is a one-step process, W14 → P7 + CO, with the transition state TS14-P7 lying as high as 76.6 kcal/mol above W3. An analogous pathway is W16 → P7 + CO, where W16 is a different conformer of W14 produced by rotation around a C-C bond or by the reverse H migration from the CH_2 group to the CO side chain in W15. Alternatively, when the longer side chain is involved, the CO loss pathway includes two steps, W3 → W17 → P8 + CO, forming the 2-methylene-benzaldehyde radical via the highest barrier of 55.2 kcal/mol above W3 at TS3-17. Interestingly, in the secondary reactions both P7 and P8 can eliminate the second CO group forming benzyl radical P9 but the corresponding barriers are high, 47.9 and 67.4 kcal/mol. Clearly, the H shift with the CO in the longer CHCHO side chain is energetically more favorable than the analogous process in the shorter HCO side chain. Finally, intermediate W17 can undergo another 1,2-H shift from the CH_2 group to the neighboring carbon in the ring followed by the elimination of the ketenyl radical HCCO and formation of benzaldehyde P10, but this channel is not expected to be competitive due to the high barrier for the H shift. Summarizing, among different decomposition channels of W3, the W3 → W14 → W15 → P5 + CO pathway should be kinetically the most favorable one.

Next, we turn our attention to decomposition channels of W9 (Figure 4). After the ring closure to W10, a loss of the H atom from the HCO group produces coumarin (2H-chromen-2-one) P11, via a barrier of only 16.1 kcal/mol. The CO elimination pathway, W9 → W19 → P12 + CO, involving 1,2-H migration from HCO in the side chain followed by the C-C bond cleavage, is most favorable thermodynamically, but features a high, 57.4 kcal/mol, barrier at TS9-19. Another 1,2-H shift in the side chain leads from W9 to W20 and elimination of the HCO group produces 6-vinylidene-cyclohexa-2,4-dienone P13. The highest barrier on this pathway, 69.0 kcal/mol relative to W9, is found at TS9-20. Finally, the least kinetically favorable channel begins with a 1,2-H shift W9 → W21 from the side chain to the ring carbon, is followed by another 1,2-H shift W21 → W22 in the side chain, and completes with elimination of the propynal molecule forming phenoxy radical P14. The highest barrier for this channel is at TS21-22, 85.8 kcal/mol above W9. Obviously, the pathway producing coumarin + H (P11) should dominate the decomposition of W9.

Summarizing the results of the PES calculations, we conclude that the reaction outcome should depend on the competition between the direct formation of 1-H-inden-1-one C_9H_6O + OH from W1 and isomerization of this intermediate to W3 and W9 (via W2 and W8, respectively). Once W3 or W9 are produced, they are rather unlikely to rearrange back to W1 (and dissociate to the indenyl + O_2 reactants) but would preferably decompose to P5 + CO or coumarin + H (P11), respectively. The rate constant calculations in the subsequent Section allow us to validate these conclusions.

3.2. Rate constants and product branching ratios

Figure 5(a) depicts the calculated total rate constants at the high pressure limit (HP) and at finite pressures. The finite pressure rate constants show peculiar features: They are nearly independent of temperature or slightly increase with *T* at low temperatures, then sharply decrease between 700 and 800 K, 700 and 800 K, 900 and 1000 K, 1000 and 1125 K, and 1375 and 1500 K at p = 0.03, 0.1, 1, 10, and 100 atm, respectively. At higher temperatures, the rate constants exhibit a typical Arrhenius behavior and coalesce, such that at 1500 K and above the total rate constant is independent of pressure in the considered p-range. These interesting features can be traced to the structure of the PES and are similar to the behavior of the C_5H_5 + O_2 total rate constant calculated in our previous work.[33] Alike to the C_5H_5 + O_2 reaction, the reaction of indenyl + O_2 at low temperatures proceeds only to the formation and collisional stabilization of the initial complex W1. The barriers on the W1 → P3 + OH, W1 → W2 → W3, and W1 → W8 → W9 pathways for subsequent dissociation/isomerization of W1 are significantly higher than that in the reverse direction back to the reactants and hence these channels are not competitive until the temperature becomes high enough. Therefore, in the initial low-temperature range the reaction flux goes nearly exclusively to W1. At a certain temperature (between 700 and 800 K, 700 and 800 K, 900 and 1000 K, 1000 and 1125 K, and 1375 and 1500 K at p = 0.03, 0.1, 1, 10, and 100 atm, respectively), reverse dissociation W1 → indenyl + O_2 overcompetes collisional stabilization of W1 and the intermediate merges/equilibrates with the reactants. As a result, the overall reaction rate constant sharply drops. At temperatures above 800, 800, 1000, 1125, and 1500 K at p = 0.03, 0.1, 1, 10, and 100 atm, respectively, W1 can no longer be collisionally stabilized as it equilibrates with the reactants and the reaction channels indenyl + O_2 → P3 + OH, indenyl + O_2 → W2 → W3, and indenyl + O_2 → W8 → W9 with subsequent decomposition of W3 and W9 become dominant. Above 1500 K, the rate constant is pressure-independent because none of the intermediates is collisionally stabilized and bimolecular products are formed either directly from the reactants (P3 + OH) or via W3 or W9. To further illustrate this behavior,

we carried out RRKM-ME calculations for the two following simplified systems: (1) only the initial reaction step, indenyl + O_2 → W1 via TS0-1, excluding all other intermediates, transition states, and products; (2) the entire reaction system excluding W1, W2, W8, TS0-1, TS1-2, and TS1-8 and connecting TS2-3, TS8-9, and TS1-P3 directly to the indenyl + O_2 reactants in the reverse direction, thus effectively merging W1, W2, and W8 with the reactants. The results are shown in Fig. 5(b). For the simplest indenyl + O_2 → W1 system, W1 can survive (until it equilibrates with the reactants) up to the same temperatures as in the whole system. Moreover, the calculated indenyl + O_2 → W1 rate constants (i.e., those for collisional stabilization of W1) computed at different pressures are also exactly the same as those obtained from the master equation solution for the whole system. This means that in the low-temperature regime the absolute eigenvalue is effectively equal to the association rate constant to form W1 from the reactants. In the system where W1, W2, and W8 are excluded, the total rate constant is independent of pressure and shows a smooth Arrhenius behavior (Fig. 5(b)). At temperatures above 800, 900, 1000, 1125, and 1500 K, the rate constant for this simplified system nearly coincides with the rate constants computed for the whole system at p = 0.03, 0.1, 1, 10, and 100 atm, respectively. This result indicates that in the high-temperature regime the presence of the shallow entrance wells W1, W2, and W8 does not affect the total rate constant with the reaction leading exclusively to various bimolecular products. The switch between the two temperature regimes occurs at the temperature at which W1 merges with reactants, i.e. when CSE for the reverse dissociation of W1 reaches IERE. In principle, one can determine this switching temperature at a particular pressure by running the master equation calculations on a fine temperature grid but this is beyond our interest in the present work. It is also worth noting that the lowest eigenvalue in the system is clearly separated from IEREs (see Figure S2 in ESI), which makes the derivation of the phenomenological rate constants for the bimolecular products in the high-temperature regime unambiguous.

When only the W1 complex is produced exclusively in the low-temperature regime (up to 700 K at 0.03 and 0.1 atm, 900, 1000, and 1375 K at 1, 10, and 100 atm, respectively), the reverse unimolecular decomposition of W1 back to indenyl + O_2 is very fast and occurs on a nanosecond scale, with the rate constant varying from 2.0×10^{6} s^{-1} at 700 K and 0.03 atm to 3.1×10^{9} s^{-1} at 1375 K and 100 atm (Table 2). The calculated values of $K_{eq} = \frac{[W1]}{[indenyl][O_2]}$ decrease from 6.07×10^{-21} cm^3 $molecule^{-1}$ at 500 K to 2.37×10^{-24} cm^3 $molecule^{-1}$ at 1375 K. Taking the concentration of O_2 corresponding to p = 1 atm of air (from ~3×10^{18} to 1×10^{18} molecule cm^{-3} in the 500-1375 K temperature range), we obtain the $\frac{[W1]}{[indenyl]}$ ratio from 1.87×10^{-3} to 2.66×10^{-6} (Fig. 5(c)), which means that the W1 complex and hence the indenyl + O_2 reaction are not expected to

play any significant role in the low-temperature regime considered here. Therefore, one can simply neglect the formation of W1 and exclusively consider the formation of bimolecular products, which can be effectively evaluated using the rate constant for the simplified system where W1, W2, and W8 are excluded (the red line in Fig. 5(b)). Still, the total rate constant to form bimolecular products is very low, under 10^{-20} cm^3 molecule^{-1} s^{-1} nearly up to 800 K, and hence the indenyl + O_2 reaction in this temperature range can be ignored for all practical purposes. At higher temperatures, the rate constant is still low and exceeds 1.0×10^{-15} cm^3 molecule^{-1} s^{-1} only above 2000 K. The reaction is predicted to predominantly produce 1-H-inden-1-one (P3) + OH with minor products being P5 + CO or coumarin (P11) + H (Table 3 and Fig. 5(d)). At 0.03 and 0.1 atm, the branching ratio of P3 increases from 61.4% to 79.7% in the T = 800-2500 K range, whereas that of P5 decrease from 32.0% to 12.0%, and the yield of P11 remains nearly steady at 7-6%. The branching ratios are nearly independent of pressure, except the bimolecular products take over the stabilization of W1 at higher temperatures with increasing pressure, in particular at 1000, 1125, and 1500 K at 1, 10, and 100 atm, respectively. The same is true for the rate constants for the individual bimolecular product channels. Fig. 5(d) shows the plots of their values identical at 0.03 and 0.1 atm, but they are also valid for the pressures of 1, 10, and 100 atm beginning from the temperatures of 1000, 1125, and 1500 K, respectively. The plots show a typical Arrhenius behavior and can be fitted with modified Arrhenius expressions $k = AT^{\alpha}\exp(-E_a/RT)$ with the parameters presented in Table 4.

It is informative to compare the calculated total rate constants for indenyl + O_2 and C_5H_5 + O_2 [33] reactions for the formation of bimolecular products in the high-temperature range and those for the main reaction channels forming 1-H-inden-1-one + OH and cyclopentadienone + OH, respectively (Fig. 5(d)). This comparison shows that the C_5H_5 + O_2 reaction overall is from a factor of 5.6 to a factor of 8.4 faster than indenyl + O_2 and the formation of cyclopentadienone is from a factor of 4.7 to a factor of 8.8 faster than the formation of 1-H-inden-1-one + OH. In part, this difference can be explained by the higher reaction path degeneracy (by a factor of 2.5) for C_5H_5 where pseudorotation makes all 5 C atoms equivalent for the O_2 attack vs. indenyl where only two symmetric atoms C2 and C4 with the highest spin density represent the most favorable sites for the approach of O_2. The rest of the difference in the rate constants can be attributed to the lower vibrational frequency in the critical transition state for the 1,3-H shift from C to O in W1 (TS1-P3 in the present system) corresponding to a torsional mode, 32 cm^{-1} in the C_5H_5 + O_2 system vs. 71 cm^{-1} for indenyl + O_2. Qualitatively, the presence of the extra six-member ring makes this critical transition state more rigid and hence the decrease of the rate constant.

4. Conclusions

Ab initio/RRKM-ME calculations of the PES, rate constants, and product branching ratios for the indenyl + O_2 reaction show that the reaction may be significant only in the high-temperature regime, at the temperatures above 800, 800, 1000, 1125, and 1500 K at p = 0.03, 0.1, 1, 10, and 100 atm, respectively. The prevailing reaction channel leads to the 1-H-inden-1-one + OH products, which are formed via the 1,3-H shift from C to O in the initial association complex W1 accompanied by OH elimination through a high barrier of 25.6 kcal/mol. The total rate constant of the indenyl + O_2 reaction leading to bimolecular products is pressure independent and increases with temperature from 2.1×10^{-20} cm^3 molecule^{-1} s^{-1} at 800 K (at 0.03 and 0.1 atm) to 6.7×10^{-15} cm^3 molecule^{-1} s^{-1} at 2500 K. The branching ratio of 1-H-inden-1-one + OH increases with temperature from ~61% to ~80%, with P5 + CO (32-12%) and coumarin + H (7-6%) being significant minor products. Nevertheless, the indenyl + O_2 reaction is rather slow to play a substantial role in the oxidation of the five-member ring in indenyl as the rate constant exceeds 1.0×10^{-15} cm^3 molecule^{-1} s^{-1} only at temperatures above 2000 K.

The present results corroborate our previous conclusion that molecular oxygen is not an efficient oxidizer of a five-member ring made based on the studies of the C_5H_5 + O_2 reaction[33] and kinetic modeling.[16] We have also found earlier that atomic oxygen oxidizes the isolated five-member ring much more efficiently than O_2[16,35,37] and recently demonstrated that the reactions with the O atom rapidly destroy embedded five-member rings in polycyclic aromatic $C_{15}H_9$ radicals.[57] It is therefore important to continue the study of indenyl oxidation by considering the indenyl + O reaction on the C_9H_7O PES. This PES will be also relevant to the 1-H-inden-1-one + H reaction, which, similar to cyclopentadienone + H,[35] may destroy the 1-H-inden-1-one molecule and thus complete the indenyl oxidation process initiated by indenyl + O_2. The studies of the C_9H_7O surface in relation to these two reactions are currently underway in our group and will be the subject of our future publication.

ACKNOWLEDGEMENTS

This work was supported by the by the Ministry of Education and Science of the Russian Federation No. 14.Y26.31.0020 to Samara University and in part by the US Department of Energy, Basic Energy Sciences Grant DE-FG02-04ER15570 to Florida International University. We thank Mr. Karyasov for some preliminary calculations of the potential energy surface.

Electronic Supplementary Information Available: Figure S1 – comparison of rate constants for the phenoxy (P14) + propynal and CO loss (P7/P8) channels calculated in the present work with those proposed by Lindstedt et al. in Ref. 15; Figure S2 – (a) the ratios of eigenvalue over the relaxation limit for six lowest eigenvalues from the master equation solution as functions of temperature at the lowest pressure of 0.01 atm; (b) The ratio of the lowest eigenvalue over the relaxation limit from the master equation solution as a function of temperature at various pressure in the 0.01 – 100 atm range; Table S1 – calculated rate constants (in cm^3 $molecule^{-1}$ s^{-1}) for individual bimolecular reaction channels; and Table S2 – calculated branching ratios for individual bimolecular reaction channels.

Table 1. Comparison of relative energies of various intermediates and transition states in the indenyl + O_2 reaction calculated in the present work and in Ref. 15.

Species	E_{rel}(G3(MP2,CC)), kcal/mol[a]	E_{rel}(G3MP2B3), kcal/mol[b]
$C_9H_7 + O_2$	0.0	0.0
TS0-1	2.8	6.5
W1	-13.7	-8.0
TS1-2	13.0	14.4
W2	-3.7	-0.2
TS2-3	23.5	28.7
W3	-81.5	-68.1
TS3-17	-26.3	-23.7
W17	-78.1	-69.8
TS17-P8	-60.0	-58.4
P8 + CO	-74.6	-68.8
TSP8-P9 + CO	-7.2	-7.3
P9 (benzyl) + 2CO	-74.1	-69.8
TS17-18	-6.3	-13.3
W18	-51.3	-51.6
TS18-P10	-28.2	-29.2
P10 (benzaldehyde) + HCCO	-35.6	-33.4
TS1-8	18.6	21.3
W8	10.4	13.5
TS8-9	25.8	30.3
W9	-63.7	-58.8
W21	-25.5	-21.4
TS21-22	22.1	25.1
W22	-24.3	-20.3
TS22-P14	-6.5	-2.4
P14 (phenoxy + propynal)	-22.0	-20.2

[a]Present work.
[b]From Ref. 15.

Table 2. Calculated rate constants for the formation (collisional stabilization) of complex W1 and its decomposition back to the indenyl + O_2 reactants.

	indenyl + O_2 → W1, cm^3 $molecule^{-1}$ s^{-1}					W1 → indenyl + O_2, s^{-1}				
T, K	0.03 atm	0.1 atm	1 atm	10 atm	100 atm	0.03 atm	0.1 atm	1 atm	10 atm	100 atm
500	4.23E-16	5.44E-16	6.60E-16	6.83E-16	6.85E-16	6.99E+04	8.96E+04	1.09E+05	1.13E+05	1.13E+05
600	3.71E-16	6.08E-16	1.03E-15	1.19E-15	1.22E-15	5.76E+05	9.24E+05	1.55E+06	1.78E+06	1.82E+06
700	2.36E-16	4.87E-16	1.23E-15	1.77E-15	1.90E-15	1.99E+06	3.72E+06	8.67E+06	1.23E+07	1.32E+07
800			1.19E-15	2.28E-15	2.71E-15			2.70E+07	4.87E+07	5.76E+07
900			9.79E-16	2.60E-15	3.60E-15			5.95E+07	1.31E+08	1.77E+08
1000				2.68E-15	4.50E-15				2.74E+08	4.25E+08
1125					5.51E-15					9.84E+08
1250					6.30E-15					1.86E+09
1375					6.74E-15					3.06E+09

Table 3. Calculated branching ratios of bimolecular products of the indenyl + O_2 reaction.[a]

T, K	1-H-inden-1-one (P3) + OH	P5 + CO	coumarin (P11) + H
800	61.37%	31.96%	6.59%
900	63.74%	29.08%	7.09%
1000	65.78%	26.66%	7.44%
1125	67.97%	24.17%	7.69%
1250	69.83%	22.14%	7.81%
1375	71.43%	20.44%	7.84%
1500	72.81%	18.99%	7.80%
1650	74.26%	17.52%	7.67%
1800	75.52%	16.25%	7.49%
2000	76.95%	14.81%	7.16%
2250	78.45%	13.29%	6.63%
2500	79.70%	11.99%	5.97%

[a]The values are given for the pressures of 0.03 and 0.1 atm but they are also valid at p = 1, 10, and 100 atm at temperatures of, respectively, 1000, 1125, and 1500 K and above.

Table 4. Parameters of fitted modified Arrhenius expressions $k = A*T^{\alpha}*\exp(-E_a/RT)$ for bimolecular products channels in the indenyl + O_2 reaction. Pre-exponential factors A are in cm^3 mol^{-1} s^{-1} and E_a are in cal mol^{-1}.[a]

Reaction channel	A	α	E_a
1-H-inden-1-one (P3) + OH	3739.2	2.3701	24090
P5 + CO	1.70E+06	1.3424	23940
coumarin (P11) + H	6.40E+07	0.87946	27315
total, bimolecular channels	6691.6	2.3128	23629

[a]The expressions are applicable at the following temperature ranges at various pressures: 0.03 and 0.1 atm – 800-2500 K, 1 atm – 1000-2500 K, 10 atm – 1125-2500 K, and 100 atm – 1500-2500 K.

Figure Captions

Figure 1. Designation of atoms in the chemical structure of indenyl + O_2.

Figure 2. Potential energy diagram for the indenyl + O_2 reaction calculated at the G3(MP2,CC)//B3LYP/6-311G(d,p) level of theory: entrance channels, OH elimination, and decomposition of W3 and W9 to C_8H_7 + CO_2. All relative energies are shown in kcal/mol relative to the initial reactants.

Figure 3. Potential energy diagram for the indenyl + O_2 reaction calculated at the G3(MP2,CC)//B3LYP/6-311G(d,p) level of theory: various channels of decomposition of W3. All relative energies are shown in kcal/mol relative to the initial reactants.

Figure 4. Potential energy diagram for the indenyl + O_2 reaction calculated at the G3(MP2,CC)//B3LYP/6-311G(d,p) level of theory: various channels of decomposition of W9. All relative energies are shown in kcal/mol relative to the initial reactants.

Figure 5. Calculated rate constants for the indenyl + O_2 reaction: (a) the total rate constant at various pressures and at the high-pressure limit (HP); (b) black lines show association rate constants computed for the simplified indenyl + $O_2 \rightarrow$ W1 system – they appeared to be identical to the total rate constant calculated for the whole system in the low-temperature regime, red line is the total rate constant computed for a simplified system excluding W1, W2, and W8 (see text for more detail) – only bimolecular products are formed in this system and the rate constant is independent of pressure, blue lines show the total rate constant computed for the whole system in the high-temperature regime; (c) unitless concentration ratio $\frac{[W1]}{[indenyl]}$ calculated from the equilibrium constant for the indenyl + $O_2 \rightarrow$ W1 reaction assuming concentrations of O_2 corresponding to p = 1 atm of air; (d) rate constants for individual bimolecular channels (identical at 0.03 and 0.1 atm). The values shown on the plots are also valid at higher pressures of 1, 10, and 100 atm beginning from the temperatures of 1000, 1125, and 1500 K, respectively. Rate constants for the C_5H_5 + O_2 reaction from Ref. 33 are shown for comparison.

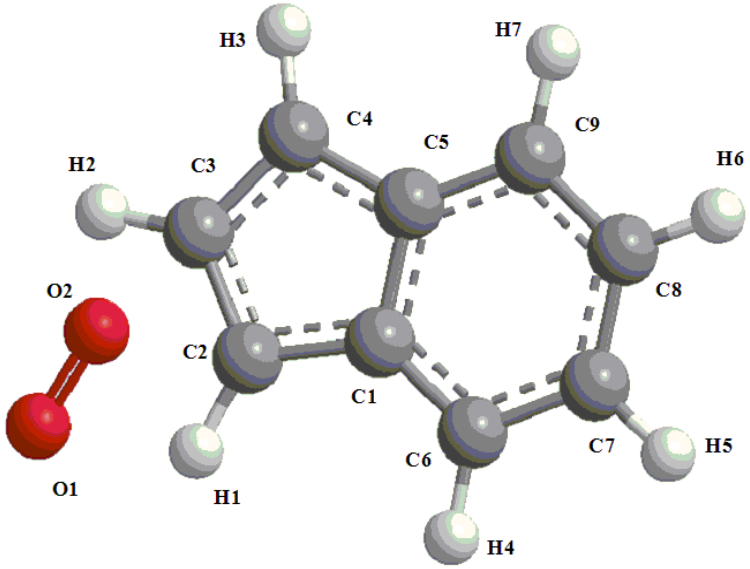

Figure 1

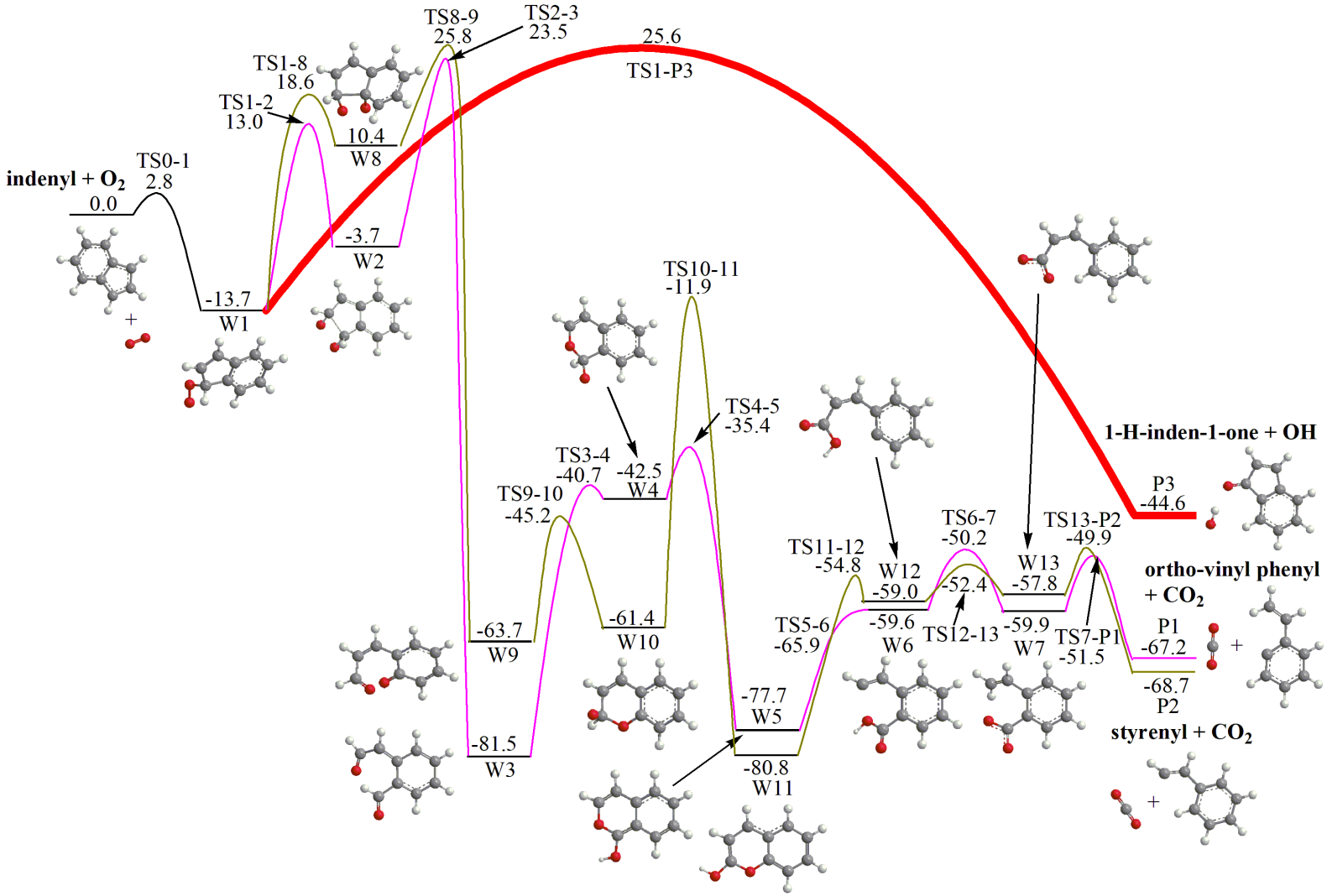
indenyl + O2
0.0
TS0-1
2.8
-13.7
W1
TS1-2
13.0
TS1-8
18.6
10.4
W8
TS8-9
25.8
TS2-3
23.5
25.6
TS1-P3
-3.7
W2
TS10-11
-11.9
TS4-5
-35.4
TS3-4
-40.7
-42.5
W4
TS9-10
-45.2
-63.7
W9
-61.4
W10
-81.5
W3
-77.7
W5
-80.8
W11
TS11-12
-54.8
W12
-59.0
TS6-7
-50.2
-52.4
W13
-57.8
TS13-P2
-49.9
TS5-6
-65.9
-59.6
W6
TS12-13
-59.9
W7
TS7-P1
-51.5
P3
-44.6
1-H-inden-1-one + OH
ortho-vinyl phenyl
+ CO2
P1
-67.2
-68.7
P2
styrenyl + CO2

Figure 2

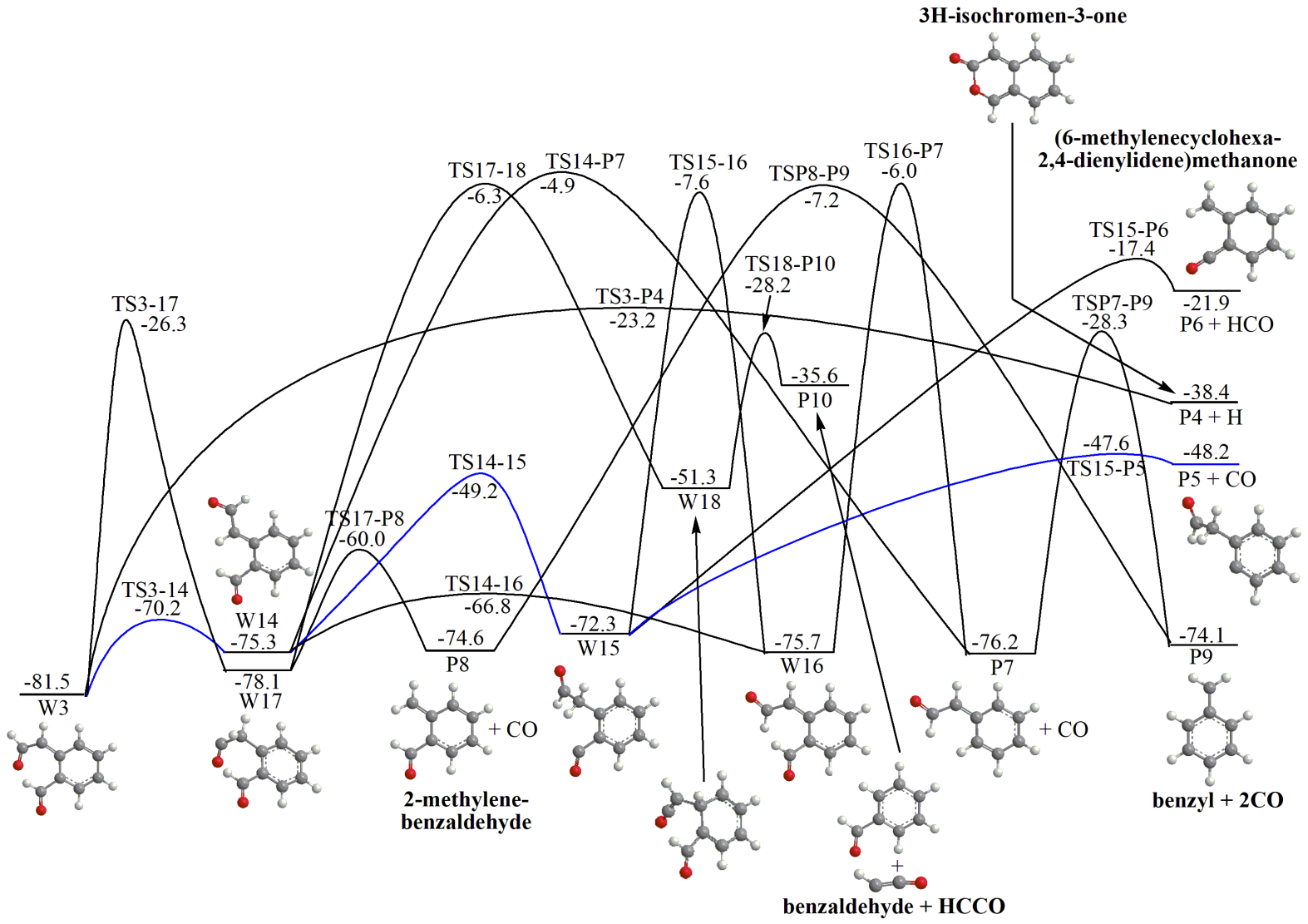
3H-isochromen-3-one
(6-methylenecyclohexa-
2,4-dienylidene)methanone
TS17-18
-6.3
TS14-P7
-4.9
TS15-16
-7.6
TSP8-P9
-7.2
TS16-P7
-6.0
TS15-P6
-17.4
-21.9
P6 + HCO
TS18-P10
-28.2
TS3-17
-26.3
TS3-P4
-23.2
TSP7-P9
-28.3
-35.6
P10
-38.4
P4 + H
-47.6
TS15-P5
-48.2
P5 + CO
TS14-15
-49.2
-51.3
W18
TS17-P8
-60.0
TS3-14
-70.2
TS14-16
-66.8
W14
-75.3
-72.3
W15
-74.6
P8
-75.7
W16
-76.2
P7
-74.1
P9
-81.5
W3
-78.1
W17
+ CO
+ CO
2-methylene-
benzaldehyde
benzyl + 2CO
benzaldehyde + HCCO

Figure 3

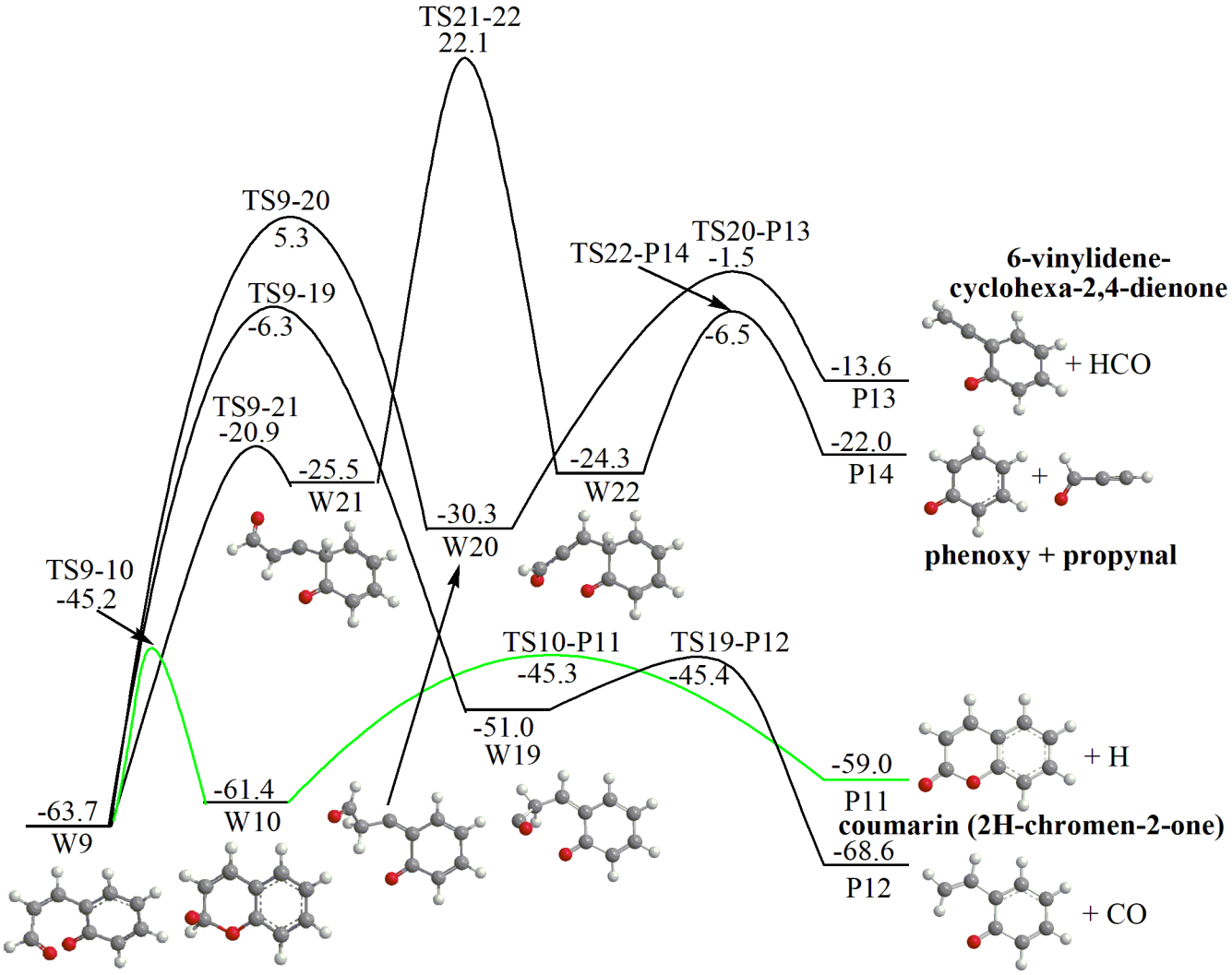
TS21-22
22.1
TS9-20
5.3
TS20-P13
-1.5
TS22-P14
TS9-19
-6.3
-6.5
6-vinylidene-
cyclohexa-2,4-dienone
-13.6
P13
+ HCO
TS9-21
-20.9
-22.0
P14
-25.5
W21
-24.3
W22
+
-30.3
W20
phenoxy + propynal
TS9-10
-45.2
TS10-P11
-45.3
TS19-P12
-45.4
-51.0
W19
-59.0
P11
+ H
-61.4
W10
coumarin (2H-chromen-2-one)
-63.7
W9
-68.6
P12
+ CO

Figure 4

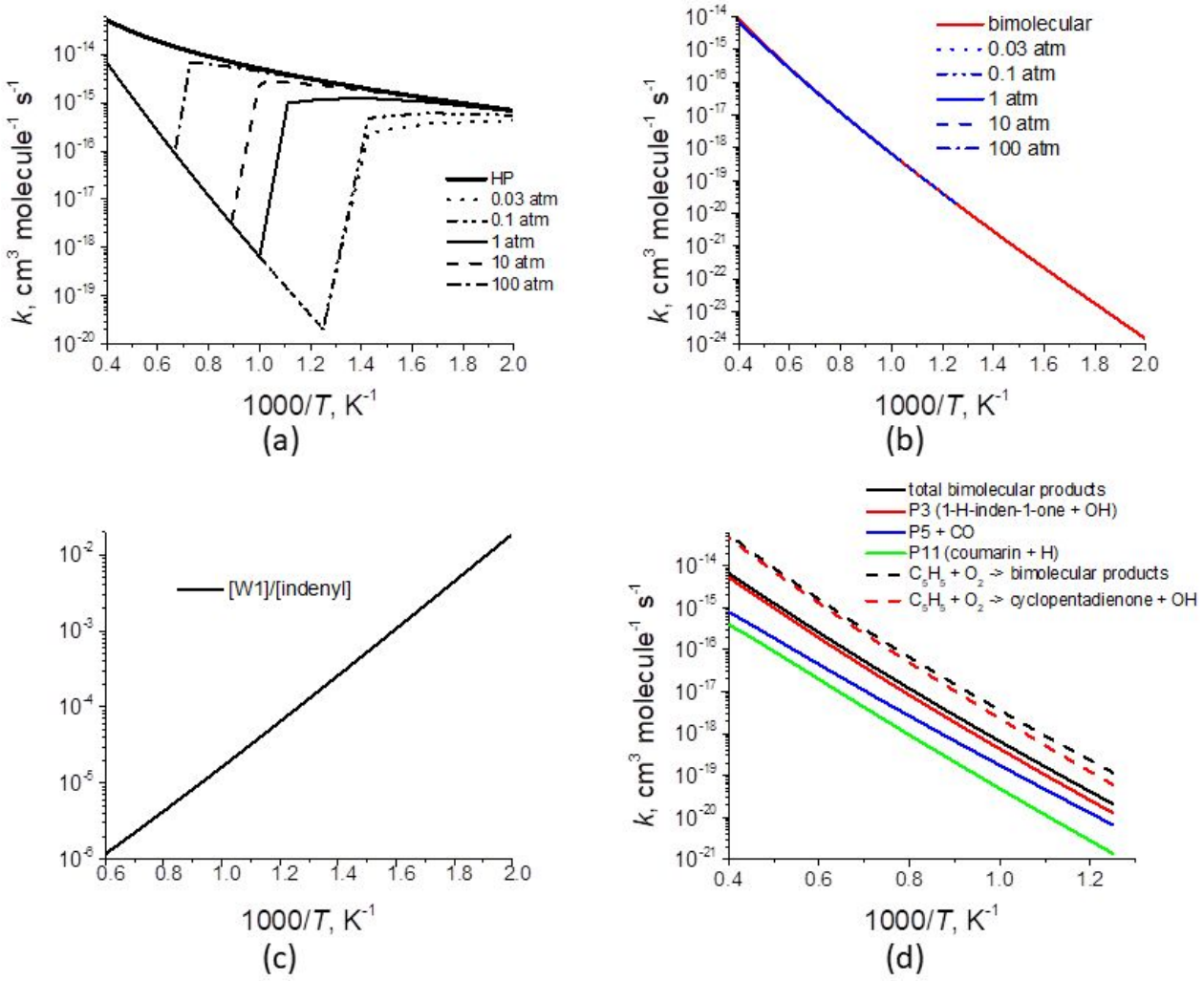
k, cm3 molecule-1 s-1
1000/T, K-1
HP
0.03 atm
0.1 atm
1 atm
10 atm
100 atm
(a)
bimolecular
0.03 atm
0.1 atm
1 atm
10 atm
100 atm
(b)
[W1]/[indenyl]
(c)
total bimolecular products
P3 (1-H-inden-1-one + OH)
P5 + CO
P11 (coumarin + H)
C5H5 + O2 -> bimolecular products
C5H5 + O2 -> cyclopentadienone + OH
(d)

Figure 5

References

1 H. Richter and J. B. Howard, *Prog. Energy Combust. Sci*., 2000, **26**, 565–608.

2 M. Frenklach, *Phys. Chem. Chem. Phys*., 2002, **4,** 2028–2037.

3 A. Alhamdow, C. Lindh, J. Hagberg, P. Graff, H. Westberg, A. M. Krais and K. Broberg, *Carcinogenesis*, 2018, **1**, 10.

4 M.R. Kholghy, G.A. Kelesidis and S.E. Pratsinis, *Phys. Chem. Chem. Phys*., 2018, **20**, 10926-10938.

5 M. Frenklach, *Combust. Flame*, 2019, **201**, 148-159.

6 J. Bouwman, A. Bodi and P. Hemberger, *Phys. Chem. Chem. Phys*., 2018, **20**, 29910-29917.

7 L. Zhao, R. I. Kaiser, B. Xu, U. Ablikim, M. Ahmed, M. V. Zagidullin, V. N. Azyazov, A. H. Howlader, S. F. Wnuk and A. M. Mebel, *J. Phys. Chem. Lett.*, 2018, **9**, 2620-2626.

8 H. Huang, J. Zhu, D. Lv, Y. Wei, Z. Zhu, B. Yu and Y. Chen, *Energy*, 2018, **165**, 90-105.

9 A. Eremin and E. Mikheyeva, *Combust. Sci. Technol*., 2018, ASAP Article, DOI:10.1080/00102202.2018.1551892.

10 N. Fedik and A. I. Boldyrev, *J. Phys. Chem. A*, 2018, **122**, 8585-8590.

11 M. L. Botero, Y. Sheng, J. Akroyd, J. Martin, J. A. Dreyer, W. Yang and M. Kraft, *Carbon*, 2019, **141**, 635-642.

12 P. Liu, Z. Li, A. Bennett, H. Lin, S. M. Sarathy and W. L. Roberts, *Combust. Flame*, 2019, **199**, 54-68.

13 P. Liu, Z. Li and W. L. Roberts, *Proc. Combust. Inst.*, 2019, **37***,* 977-984.

14 D. A. Knyazkov, T. A. Bolshova, A. M. Dmitriev, A. G. Shmakov, O. P. Korobeinichev, *Energy Fuels*, 2018, ***32***, 2397-2406.

15 R. P. Lindstedt, V. Markaki and R. K. Robinson, in *Combustion Generated Fine Carboneceous Particles*, ed. H. Bockhorn, A. D'Anna, A. F. Sarofim and H. Wang, Scientific Publishing, Karlsruhe, ISBN 978-3-86644-441-6, 2009, pp. 483-505.

16 M. Frenklach, Z. Liu, R. I. Singh, G. R. Galimova, V. N. Azyazov and A. M. Mebel, *Combust. Flame*, 2018, **188**, 284-306.

17 S. J. Harris, *Combust. Sci. Technol*., 1990, **72**, 67-77.

18 Z. A. Mansurov, *J. Eng. Phys. Thermophys*., 2011, **84**, 125-159.

19 B. S. Haynes and H. G. Wagner, *Prog. Energy Combust. Sci*., 1981, *7*, 229-273.

20 L. Zhu, X. Shi, Y. Sun and Q. Zhang, *Chemosphere*, 2017, **189**, 265-276.

21 S. K. Jain, A. S. Badhe and S. K. Aggarwal, in *2018 AIAA Aerospace Sciences Meeting*, 2018, p. 1713.

22 J. Z. Yang, L. Zhao, J. H. Cai, F. Qi and Y. Y. Li, *Chin. J. Chem. Phys*., 2013, **26**, 245-251.

23 J. B. Kim, M. L. Weichman, T. I. Yacovitch, C. Shih and D.M. Neumark, *J. Chem. Phys.*, 2013, **139**, 104301.

24 C. Wentrup, H. W. Winter and D. Kvaskoff, *J. Phys. Chem. A*, 2015, **119**, 6370-6376.

25 A. M. Mebel, A. Landera and R. I. Kaiser, *J. Phys. Chem. A*, 2017, **121**, 901−926.

26 V. Dias, H. M. Katshiatshia and H. Jeanmart, *Combust. Flame*, 2011, **158**, 848-859.

27 R. G. Butler and I. Glassman, *Proc. Combust. Inst.*, 2009, **32**, 395–402.

28 H.-B. Xie, C. Li, N. He, C. Wang and S. Zhang, J. Chen, *Environ. Sci. Technol*., 2014, **48**, 1700-1706.

29 Q. Yu and H.-B. Xie, J. Chen, *Sci. Total Environ*., 2016, **571**, 1105-1114.

30 A. M. Mebel, Y. Georgievskii, A. W. Jasper and S. J. Klippenstein, *Faraday Discuss*., 2017, **195**, 637-670.

31 F. Zhang, R. I. Kaiser, V. V. Kislov, A. M. Mebel, A Golan and M. Ahmed, *J. Phys. Chem. Lett*., 2011, **2**, 1731−1735.

32 D. S. N. Parker, F. Zhang, R. I. Kaiser, V. V. Kislov and A.M. Mebel, *Chem. - Asian J.*, 2011, **6**, 3035−3042.

33 A. D. Oleinikov, V. N. Azyazov and A. M. Mebel, *Combust. Flame*, 2018, **191,** 309-319.

34 G. R. Galimova, V. N. Azyazov and A. M. Mebel, *Combust. Flame*, 2018, **187**, 147-164.

35 A. R. Ghildina, A. D. Oleinikov, V. N. Azyazov and A.M. Mebel, *Combust. Flame*, 2017, **183**, 181-193.

36 A. R. Ghildina, A. M. Mebel and V.N. Azyazov, *Bull. Lebedev Phys. Inst.*, 2018, **45**, 291-294.

37 A. R. Ghildina, A. M. Mebel, I. A. Medvedkov and V.N. Azyazov, *Combust. Expl. Shock Waves*, 2018, **54**, 9-15.

38 X. Zhong and J. W. Bozzelli, *J. Phys. Chem. A*, 1998, **102**, 3537-3555.

39 R. K. Robinson and R. P. Lindstedt, *Combust. Flame*, 2011, **158,** 666–686.

40 A. W. Jasper, K. M. Pelzer, J. A. Miller, E. Kamarchik, L. B. Harding and S. J. Klippenstein, *Science*, 2014, **346**, 1212-1215.

41 F. Xu, A. M. El-Leathy, C. H. Kim and G.M. Faeth, *Combust. Flame*, 2003, **132**, 43–57.

42 C. H. Kim, A. M. El-Leathy, F. Xu and G.M. Faeth, *Combust. Flame*, 2004, **136**, 191–207.

43 C. H. Kim, F. Xu and G.M. Faeth, *Combust. Flame*, 2008, **152**, 301–316.

44 H. Ghiassi, D. Lignell and J. S. Lighty, *Energ. Fuels*, 2017, **31**, 2236–2245.

45 A. D. Becke, *J. Chem. Phys*., 1993, **98**, 5648-5652.

46 C. Lee, W. Yang and R. G. Parr, *Phys. Rev. B*, 1988, **37**, 785-789.

47 A. G. Baboul, L. A. Curtiss, P. C. Redfern and K. Raghavachari, *J. Chem. Phys*., 1999, **110,** 7650-7657.

48 L. A. Curtiss, K. Raghavachari, P. C. Redfern, A. G. Baboul and J.A. Pople, *Chem. Phys. Lett*., 1999, **314**, 101-107.

49 M. J. Frisch, G. W. Trucks, H. B. Schlegel et al., Gaussian 09, revision B.01, Gaussian, Inc.: Wallingford, CT (2010).

50 MOLPRO, version 2010.1, a package of ab initio programs, H.-J. Werner, P. J. Knowles, G. Knizia, F. R. Manby, M. Schütz, and others, see http://www.molpro.net.

51 Y. Georgievskii and S. J. Klippenstein, Master Equation System Solver (MESS), 2015, available online at http://tcg.cse.anl.gov/papr.

52 Y. Georgievskii, J. A. Miller, M. P. Burke and S. J. Klippenstein, *J. Phys. Chem. A*, 2013, **117**, 12146-12154.

53 S. J. Klippenstein, V. S. Pande and D. G. Truhlar, *J. Am. Chem. Soc.*, 2014, **136**, 528−546.

54 J. Troe, *J. Chem. Phys*., 1977, **66**, 4745–4757.

55 A. W. Jasper and N. Hansen, *Proc. Combust. Inst*., 2013, **34,** 279–287.

56 A. W. Jasper and J. A. Miller, *J. Phys. Chem. A*, 2011, **115**, 6438–6455.

57 G. R. Galimova, V. N. Azyazov, D. P. Porfiriev and A. M. Mebel, *Chem. Phys*., 2019, **519**, 101-109.